ADVANCED FUNCTIONAL MATERIALS
www.afm-journal.de

Double Nanowires for Hybrid Quantum Devices

Thomas Kanne, Dags Olsteins, Mikelis Marnauza, Alexandros Vekris, Juan Carlos Estrada Saldaña, Sara Lorìc, Rasmus D. Schlosser, Daniel Ross, Szabolcs Csonka, Kasper Grove-Rasmussen, and Jesper Nygård**

Parallel 1D semiconductor channels connected by a superconducting strip constitute the core platform in several recent quantum device proposals that rely, for example, on Andreev processes or topological effects. In order to realize these proposals, the actual material systems must have high crystalline purity, and the coupling between the different elements should be controllable in terms of their interfaces and geometry. A strategy for synthesizing double InAs nanowires by the vapor-liquid-solid mechanism using III-V molecular beam epitaxy is presented. A superconducting layer is deposited onto nanowires without breaking the vacuum, ensuring pristine interfaces between the superconductor and the two semiconductor nanowires. The method allows for a high yield of merged as well as separate parallel nanowires with full or half-shell superconductor coatings. Their utility in complex quantum devices by electron transport measurements is demonstrated.

1. Introduction

The current progress in quantum technology goes hand-in-hand with advances in materials science.[1] Within solid state devices, hybrid semiconductor nanowires (NWs) have attracted attention as experimental model systems for quantum computing approaches, including gate-tunable superconducting qubits[2–4] and devices for studies of Majorana modes that may act as topologically protected qubits.[5,6] A number of recent proposals are based on multiple coupled nanowires, not yet realized experimentally. For example, pairs of parallel nanowires are at the core of the setup for fractional Majorana fermions that require the one-dimensionality of the individual nanowires combined with inter-wire coupling by crossed Andreev reflections.[7] The resulting "parafermions" are expected to enable topological protection on a wider set of operations than Majorana mode qubits thanks to their richer topological structure. Another interesting scenario is the topological Kondo effect[8,9] that could be realized by joining two NWs in the topological regime by a common superconducting island.

Similar double nanowire geometries could lead to tuning of Majorana regimes,[10] Majorana box qubits with projection control,[11] and other coupled bound state systems, including Andreev bound state molecules.[12,13] These proposals all serve to show that building double nanowires (DNWs) could be key for demonstrating a suite of exotic phenomena and testing hypotheses not accessible with only individual superconducting hybrid NWs.

Harnessing the material properties of DNWs would be essential since all the proposals require extremely well-defined wire geometries and interfaces, including control of the inter-wire spacing, ranging from direct contact and tunneling between the semiconductors to purely electrostatic coupling. Most single nanowire studies have been based on bottom-up synthesized III-V semiconductor nanowires, for example, InAs and InSb, normally grown by the vapor-liquid-solid (VLS) mechanism that yields single-crystal, 1D semiconductors with diameters around 100 nm. By coating these with epitaxial superconducting shells, the base materials for the single nanowire qubit schemes were formed.[2,14,15] However, assembling such nanostructures in pairs or even more complex circuits is a challenge. The incentive to grow VLS nanowires in coupled configurations has recently led to X-junction and "hashtag" devices[16–18] as well as demonstrations of 3D branched "tree" structures,[19,20] the latter not being compatible with conventional planar device manufacture.

Until now pairs of parallel, identical nanowires coupled by a superconducting layer have not been rationally synthesized. Such hybrid double nanowires would directly fit in standard device fabrication schemes, (see **Figure 1**g–i for example). However, so far, realization of DNWs has only been possible by randomly depositing NWs on a substrate and localizing pairs that stick together,[21] or by identifying nanowires

T. Kanne, D. Olsteins, M. Marnauza, A. Vekris, J. C. Estrada Saldaña, S. Lorìc, R. D. Schlosser, D. Ross, K. Grove-Rasmussen, J. Nygård
Center For Quantum Devices
Niels Bohr Institute
University of Copenhagen
Copenhagen 2100, Denmark
E-mail: thomas.kanne@nbi.ku.dk; nygard@nbi.ku.dk

M. Marnauza
Centre for Analysis and Synthesis
Lund University
Box 124, Lund 22100, Sweden

A. Vekris
Sino-Danish College (SDC)
University of Chinese Academy of Sciences
380 Huaibeizhuang, Huairou District, Beijing 101408, China

S. Csonka
Department of Physics
Budapest University of Technology and Economics and Nanoelectronics 'Momentum' Research Group of the Hungarian Academy of Sciences
Budafoki ut 8, Budapest 1111, Hungary

The ORCID identification number(s) for the author(s) of this article can be found under https://doi.org/10.1002/adfm.202107926.

DOI: 10.1002/adfm.202107926

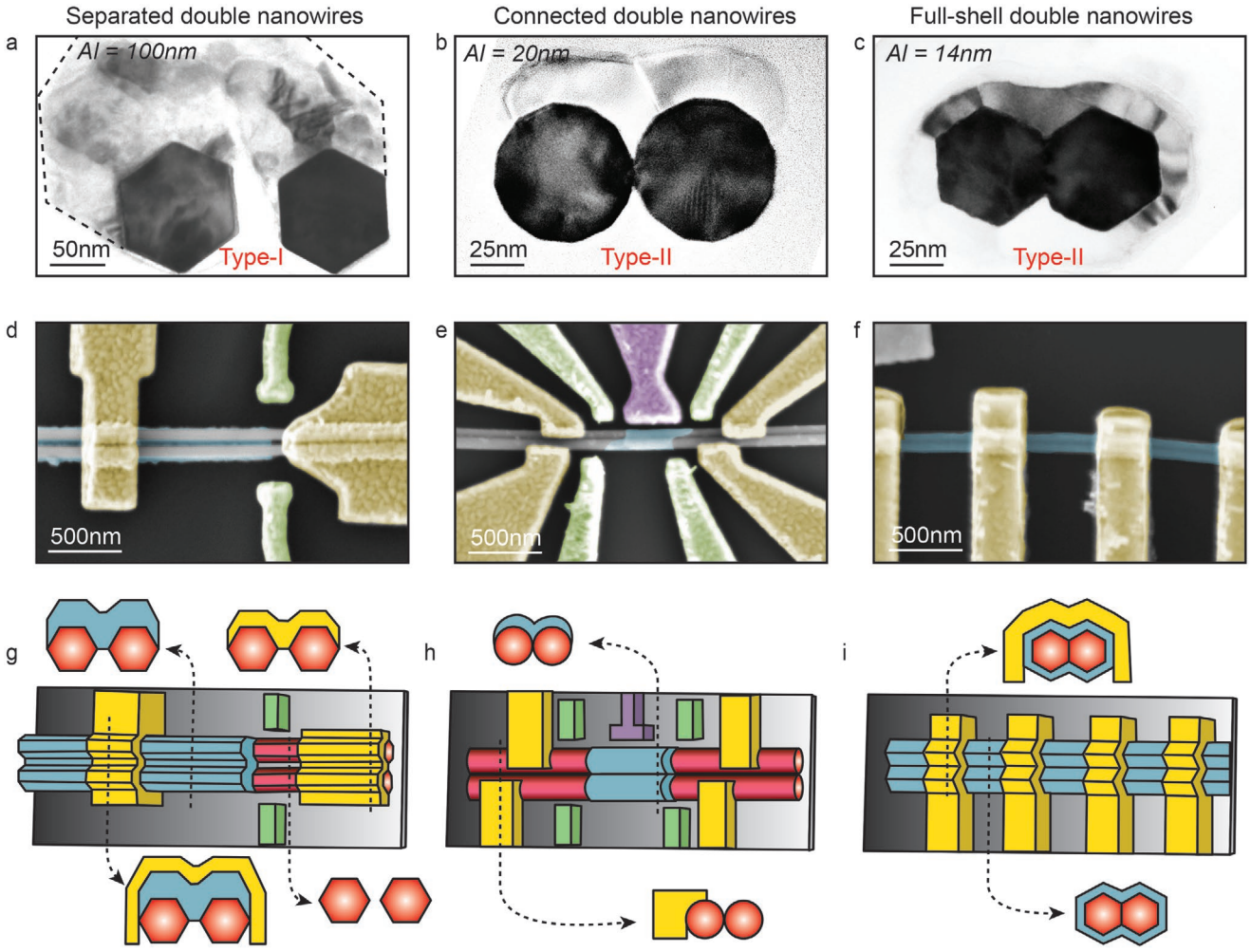

Figure 1. Double-nanowire configurations and device layouts. a–c) Transmission electron micrographs of nanowire cross sections, where pairs of parallel InAs nanowires in three different configurations are coated with an Al film, either on one side (a,b) or around the entire pair as a full shell (c). d–f) Scanning electron microscopy images of devices; gated normal nanowire-superconductor junction (d), superconducting island with four independent contacts and several gates (e), and full shell double nanowire with a full shell superconducting coating (f). g–i) Schematics reflecting the geometry of the devices in panel (d–f); with InAs nanowires (red), aluminum coatings (blue), and gold contacts and gate electrodes (yellow). For (g), the two nanowires are separated (type I) while they are directly connected in (h) and (i) (type II).

that accrete during VLS growth by accident. The first approach has recently been used for devices showing Cooper pair splitting in superconductor-DNW junctions,[22,23] but these techniques do not allow for the crucial controlled in situ deposition of an epitaxial superconducting shell.[2,15] Conversely, in situ formation of hybrid DNWs would allow for the clean, uniform superconductor–semiconductor interface needed to reach the new regimes discussed above. In this work, we show highly reliable methods for producing DNWs based on pairs of InAs nanowires positioned next to each other during VLS growth. To grow nanowires spaced from each other in a "train track" geometry (denoted type I), the growth parameters are set to yield rigid nanowires, ensuring that the separation between the nanowires remains constant from top to bottom. These structures are realized with a superconductor (Al) half-shell and full-shell configuration while still retaining a separation between the nanowires; see a cross section in Figure 1a. In a different approach (denoted type II), the growth parameters are set to yield longer and comparably less rigid nanowires. Here, the nanowire pairs connect in their upper segments before the metal deposition as van der Waals forces clamp the two nanowires together in an "Eiffel tower" configuration, yielding directly connected NWs (Figure 1b,c). The DNW geometry can be easily tuned by change of growth parameters and adjustment of the initial Au particle dimensions and inter-particle separation. Below, we describe in more detail the synthesis and design criteria behind these structures and demonstrate that they can be readily implemented in selected quantum devices (Figures 1d–f). We note that these materials have recently been exploited for studies of Andreev molecular states,[24] double quantum dot Josephson junctions[25] (Figure 1d), and Little–Parks oscillations using full-shell DNWs[26] (Figure 1f), demonstrating that ready-made DNWs are useful in functional quantum devices. Finally, we show designs that extend beyond the double-wire configurations and may enable experiments that can by no means be realized by serendipitous DNW formation.

2. Growth of Parallel Nanowires

Molecular beam epitaxy (MBE) is used to grow double InAs nanowires with a Wurtzite crystal structure along the [0001] B direction on InAs (111)B substrates. The double nanowires are grown via the VLS mechanism and catalyzed by a pair of electron-beam lithography (EBL)-defined Au particles. To facilitate growth of pairs of nanowires in very close proximity, the Au particles are engineered and patterned according to the intended inter-nanowire geometry (type I/II), while the MBE growth procedure itself is similar to one used for conventional single nanowires. To have precise control of the Au catalyst particles (disc radius r_D) and their separation (D_{Au}), multiple electron beam dot exposures ("single shots") are positioned in a pre-defined pattern with a dot separation of 20 nm. The typical disc thickness and radius is around 20 and 25–50 nm, respectively (see Supporting Information for details on Au particle formation and growth procedures). Growth of double nanowires follows largely the single nanowire growth dynamics; however, the close proximity of the nanowires reduces the contribution of adatoms to the liquid due to the shared adatom collection area on the substrate.[27] In InAs nanowire growth, the main adatom contribution consists of In atoms and thus a higher effective V/III flux ratio is attained for double nanowires. With the current growth parameters, this causes the double nanowires to be thinner compared to single nanowires. This effect can readily be counteracted in MBE by change of nominal fluxes.

Growth parameters and a comparative analysis of single and double nanowire growth are presented in Section S4, Supporting Information. After VLS growth of the semiconductor nanowires, an aluminum layer is deposited onto nanowires by electron beam evaporation in a separate metal deposition chamber connected directly to the MBE system. The evaporation of the aluminum film follows the procedure outlined in ref. [28] where a low substrate temperature ($T_{sub} \approx 120$ K) and high rate (3 Å s^{-1}) are found to ensure a pristine bi-crystal interface while maintaining a flat and continuous morphology.[14,28] The visible grain structure in the Al layers coating the double nanowires (Figure 1a–c) is similar to what is found for single nanowires[14].

Arrays of double nanowires are defined by the lithographic patterning of Au particles prior to the growth. In order to obtain various double nanowire configurations, we define fields where the separation between the centers of the Au particles D_{Au} is varied from, for example, 50 to 300 nm at intervals of 10 nm while also varying the Au disc radius. With this strategy, we find nanowires that are too far apart and therefore stand as single nanowires as well as Au particles that are too close and combine to nucleate a single nanowire. However, importantly, we ensure the formation of extended arrays of parallel nanowires with appropriate inter-nanowire spacings, independent of fluctuations between growths and minor adjustments of growth parameters.

Figure 2 shows InAs nanowires grown with varied Au particle radii and a constant initial Au-droplet center-center separation of 160 nm. To close the gap between the nanowire pairs, a thick layer (≈100 nm) of Al was deposited with an angle of ≈20° with respect to the normal of the gap between the nanowires. The scanning electron microscopy (SEM) micrographs in Figure 2c are obtained at an angle opposite to the Al deposition direction in order to highlight the morphology of the nanowires. The top row focuses on the base of the nanowires, while the bottom row reveals the shading effects on the substrate. From Figure 2, pronounced thickness-dependent bending of the nanowires is observed as seen also for single nanowires.[14,29] By examining the metal deposited on the substrate, it appears that all semiconductor nanowires grow separately

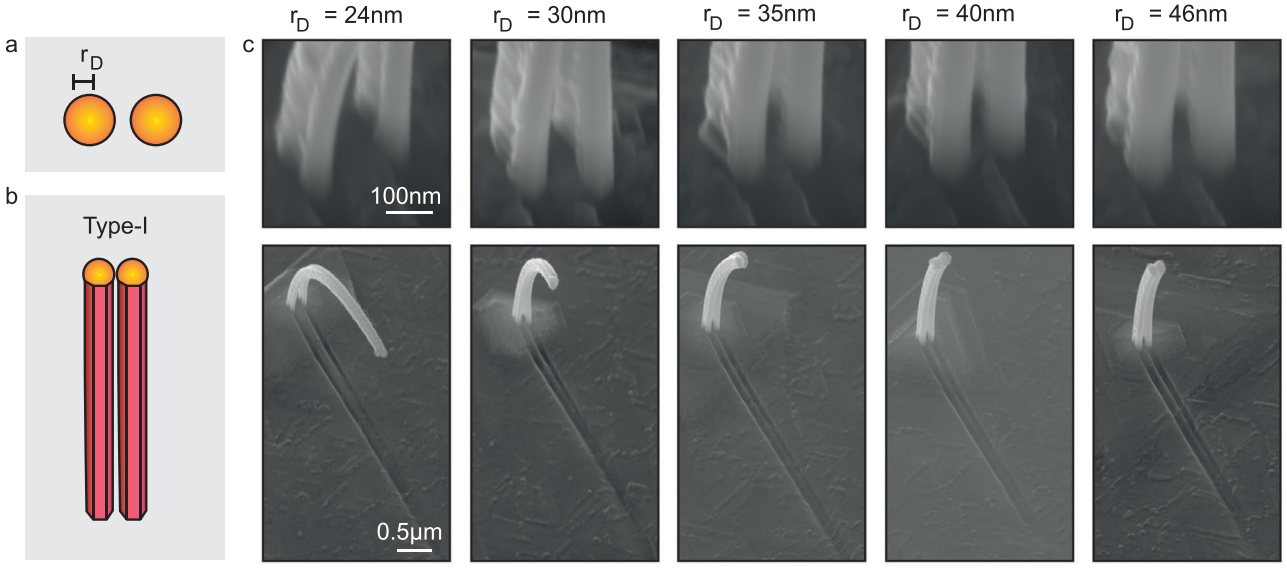

Figure 2. InAs nanowire pairs grown utilizing the type I approach. a) Initial Au particle configuration. b) Schematic of double nanowire with a constant inter-nanowire separation. c) SEM micrographs of nanowires grown with a center to center Au particle separation of D_{Au} = 160 nm and different Au disc radii r_D. Top-row micrographs show the bottom part of the nanowire pairs and the lower row shows the full nanowire system and shadows cast on the substrate during metal evaporation.

and in a later stage connect via the Al film, in accordance with transmission electron microscopy (TEM) studies of cross sections such as Figure 1a. For the specific conditions used for the growths in Figure 2, diameters greater than 80 nm yield a uniform nanowire separation, that is, type I double nanowires.

We also observe from Figure 2c that longer nanowires with smaller diameters merge near the top. These flexible nanowires[30] are accidentally clamped by van der Waals forces when vibrating in the growth chamber.

To further enhance this behavior and thus facilitate predominantly type II merged nanowires, the growth parameters are adjusted to form thinner and longer nanowires. To decrease the average nanowire diameter for the growth shown in **Figure 3**d, we increased the V/III flux ratio (≈20) by increasing the As_4 flux during the axial growth step (see Sections S4 and S5, Supporting Information, for details). This yielded nanowires with diameters of ≈50 nm for Au droplets with $r_D \approx 24$ nm and ≈130 nm for $r_D \approx 100$ nm. To fully cover the nanowires by Al, six depositions of ≈5 nm were performed with 60° rotations between each evaporation, as schematically shown in Figure 3c. Single directional evaporations are equally feasibly as shown later in Figure 5. In Figure 3d, SEM micrographs of nanowires are shown for facet-to-facet and corner-to-corner configurations (see blue and red schematics, respectively, in Figure 3c) with center-to-center Au particle separation varied from 50 to 160 nm and $r_D = 24$ nm. The initial Au particles are positioned according to the underlying crystallographic basis of the substrate to achieve the different configurations. For all separations above 50 nm, the images show consistent parallel nanowires in both configurations. A TEM micrograph of a full-shell type II cross section is shown in Figure 1c. Occasionally, internanowire spacings and nanowire dimensions are observed to differ from the intended range, and some Au particles are found missing in post-growth SEM characterization. In rare cases, the nanowires do not grow along the intended [0001]B direction. With these aberrations, we find a yield of 50–60% for type II merged nanowires as documented in Section S3, Supporting Information. For these growths, hundreds of identical double nanowires are found in numerous arrays across the growth substrates. We believe that most of the mishaps can be

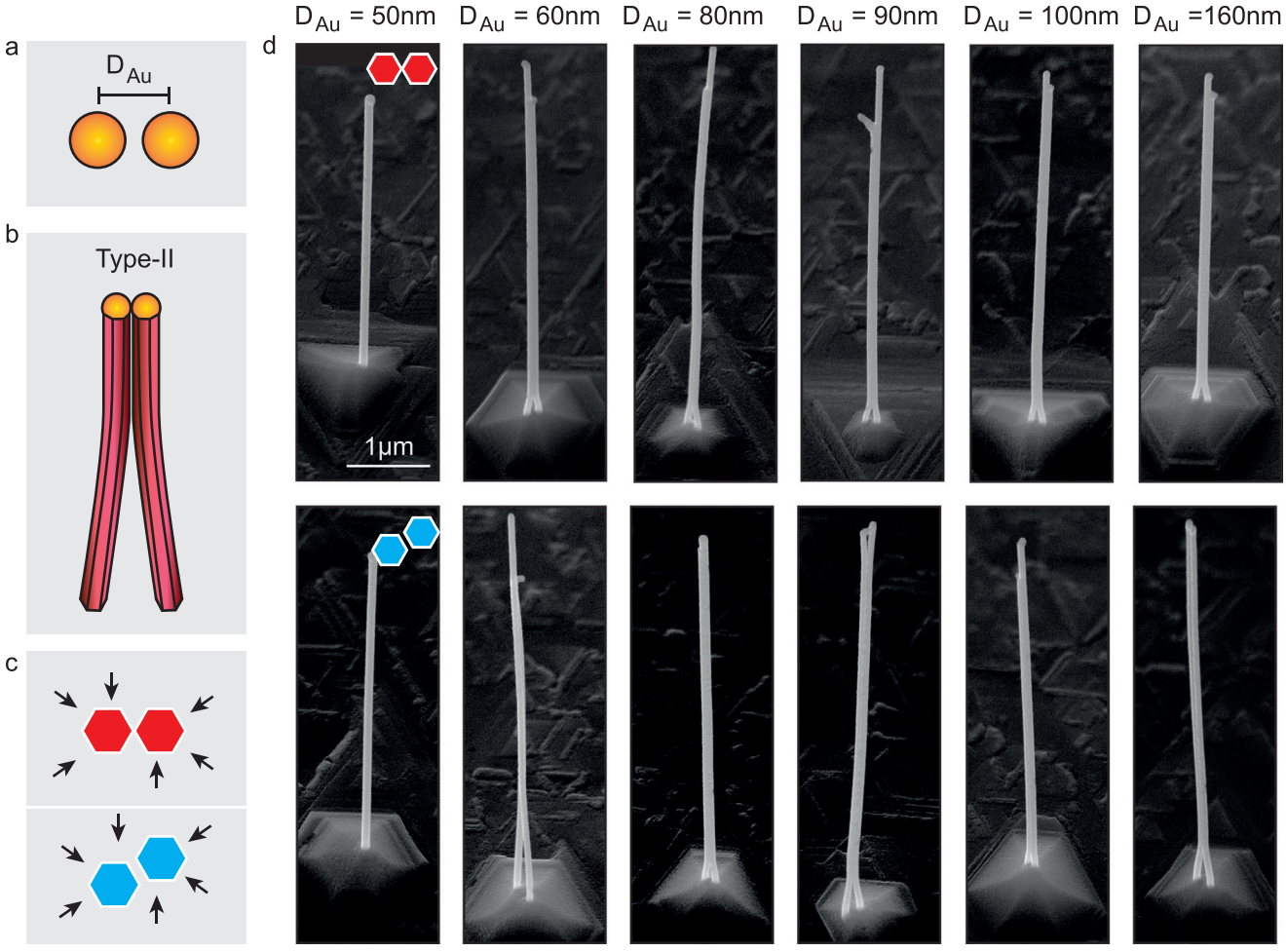

Figure 3. Parallel InAs nanowires utilizing the type II growth approach with a full shell of Al. a) The initial Au particle disk separation (D_{Au}). b) The type II merging scheme. c) Top-view schematic of a corner-to-corner (red) and a facet-to-facet (blue) configurations with an ≈27 nm full Al shell resulting from six depositions perpendicular to nanowire facets. d) SEM micrographs of nanowire pairs in the corner-to-corner and facet-to-facet configurations for Au particles formed by one single electron beam exposure and a center to center particle separation according to the text above the micrographs. The scales are all the same and noted in the first micrograph.

related to variations in the Au nanoparticle lithography process. The present work is not focused on optimization of the large scale yield; however, based on the demonstrated results we expect that near unity yield for double nanowire growth can be reached with optimization of the substrate preparation. The growth dynamics for paired InAs nanowires practically follows that of conventional single nanowires; thus, modifications of growth parameters can readily be used to control the crystal quality and nanowire dimensions, which is important for fulfilling the requirements in the proposed device designs. We find that it is easier to achieve a high yield of type II merged nanowires compared to type I. For the latter type, it is a challenge to define Au particles that can catalyze large (thick) nanowires whose rigidity prevents type II merging and yet are spaced close enough that the subsequent metal deposition can fill the gap between the vertical wires. One can overcome this by radially overgrowing nanowires that are nucleated by Au particles with a large height/diameter aspect ratio. Such particles show smaller displacement when they acquire the shape of a spherical cap at the growth temperatures. This approach is demonstrated in Section S2, Supporting Information.

3. Electrical Transport Characterization

We now turn to electrical transport characterization of the hybrid double nanowire system, focusing here on low-temperature transport measurements of two different types of devices in the quantum regime. The objective is to demonstrate that decoupled double nanowires and multi-terminal device functionalities can be achieved (more advanced functionalities are demonstrated in dedicated publications[24–26]). Prior transport experiments on parallel nanowires have been based on individual nanowires that were accidentally merged during deposition.[22,23]

In contrast, we transferred ready-made DNWs from the growth substrate to pre-patterned device substrates using a micromanipulator under an optical microscope.

The first example is a parallel double quantum dot device formed between the superconducting in situ deposited 100 nm Al and an ex situ evaporated normal metal (Ti/Au) covering both wires (Figure 1d). Prior to deposition of the normal metal, the Al on part of the nanowires has been partly removed by etching (Al etchant Transene D). **Figure 4**a shows a conceptual schematic of the resulting device, where side (g1, g2) and back gate voltage are appropriately tuned to make a superconductor (S)-parallel double quantum dot (DQD)-normal (N) device (see also Figure 1g for device schematics).[21,31] The conductance versus side gate voltage map plotted in Figure 4b shows two slopes of conductance resonances (nearly horizontal/vertical), consistent with transport through two parallel quantum dots. To address the superconducting properties of the in situ deposited Al segment, we perform bias spectroscopy along the dashed traces in Figure 4b to independently tune the occupation of each quantum dot. For both QDs, we observe clear signs of tunneling via the superconducting coherence peaks at $eV_{sd} \sim \pm 200$ μV shown in Figure 4c,d in agreement with the expected superconducting energy gap of an Al film. Importantly, the two QDs appear only weakly coupled, with an upper bound given by the width of the resonances (Figure 4b),[32] in accordance with the separated "train track" nanowire geometry (type I). Moreover, the behavior in particular for QD1 seems to reflect Yu–Shiba–Rusinov states in different coupling regimes.[33–35] The superconductor-DQD-normal metal device geometry is easily extended to S-parallel DQD-S Josephson junctions, where supercurrent and bound states behavior can be addressed.[24,25]

The second example is a superconducting island defined across the two nanowires, a geometry relevant for several device proposals in the topological and non-topological regimes.[8,9,36,37] The SEM picture in Figure 1d shows a "Tetris" island geometry (potentially relevant to decrease the overlap of Majorana end states on the island if it were in the topological regime), while the data discussed below were obtained on a rectangular island of length 330 nm. The superconducting island is defined by lithographic patterning and an etching step of the 17 nm thick Al film. Subsequently, normal metal electrodes are defined on each nanowire following standard EBL and metal deposition recipes. The device schematics is shown in Figure 4e (see also Figure 1h), where the superconducting island—in contrast to a single nanowire device—has contact to four leads. In Figure 4f,g, we show the two-terminal linear conductance of two combinations of leads (1-2, 4-1) versus side gate voltage with the other terminals floating. The traces clearly display Coulomb blockade behavior in the weakly coupled regime. This phenomenon is further confirmed by the bias spectroscopy measurements shown in Figure 4h for one of the combinations revealing Coulomb blockade diamonds. The superconducting properties cannot be deduced from this data alone, but additional measurements in a different coupling regime reveal the superconducting properties in the even–odd regime via finite bias negative differential conductance features[38] facing the odd occupation of the island (to be reported in a separate work). The demonstration of Coulomb blockade via different leads to the same superconducting island is promising for investigations of the topological Kondo effect, Majorana box qubits[11] and specific proposals based on the hybrid double nanowire geometry.[8–10,36,37,39–48] Yet other experiments addressing the transport properties of the same double nanowire materials demonstrate coupled Andreev states[24] and Yu–Shiba–Rusinov physics[25] emerging in the double nanowire Josephson junction geometry. Furthermore, the full-shell double nanowire devices such as the one represented by Figure 1c,f show Little–Parks oscillations in low-temperature transport measurements under a parallel magnetic field,[26] underlining that a broad range of quantum transport phenomena can be addressed in these parallel nanowire systems.

4. Beyond Double Nanowires

Growth substrate preparation by EBL allows the controlled fabrication of several different nanowire structures as shown in **Figure 5**. Here in situ nanowire shadowing of the subsequently deposited superconductor was furthermore implemented to allow for fabrication of hybrid devices without metal etching steps.[49] By fine tuning catalyst size and positioning via the EBL

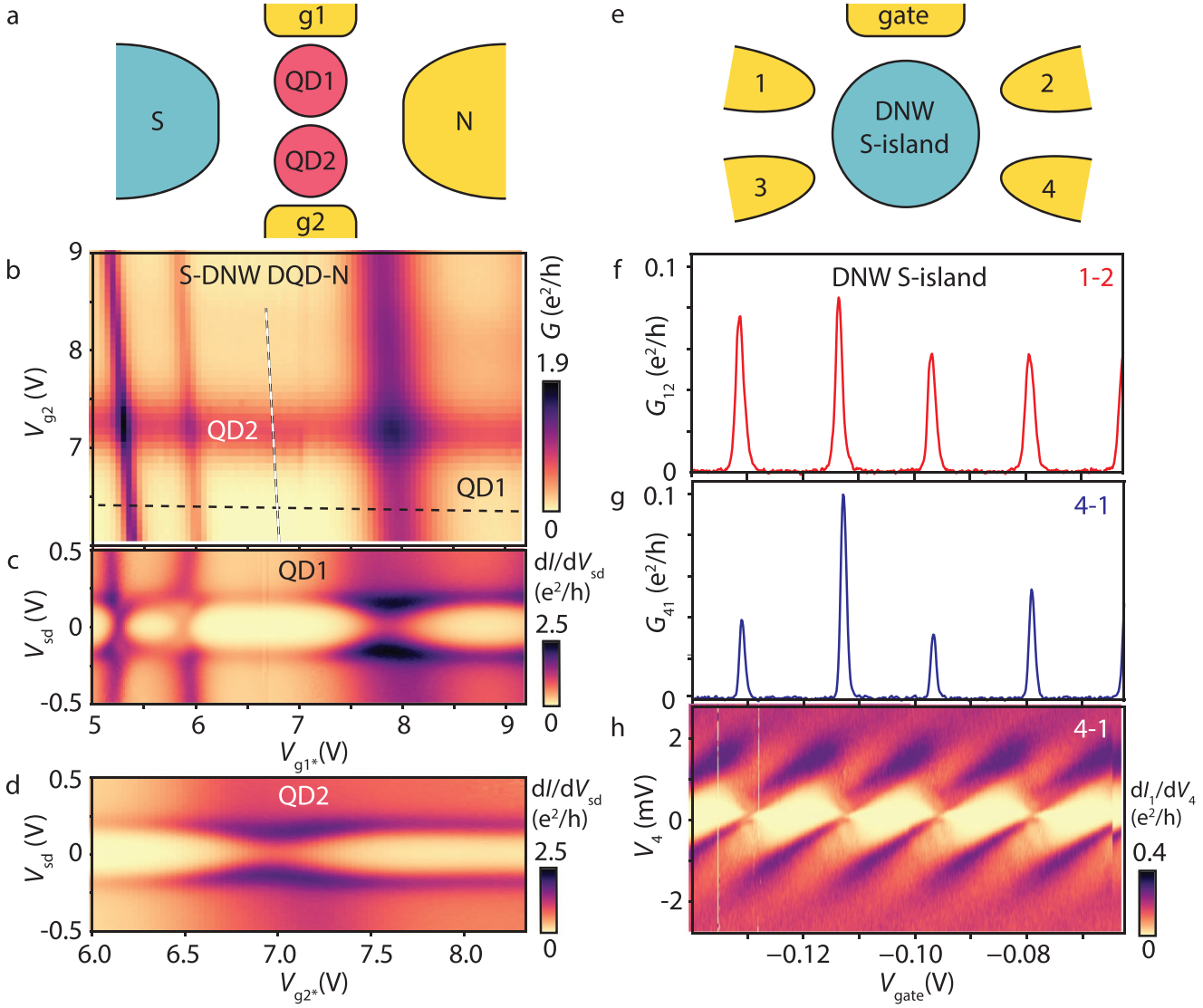

Figure 4. Electrical transport measurements of two hybrid double nanowire (DNW) devices. a) Schematic of a gated superconductor (S)-parallel double quantum dot (QD)-normal (N) device defined in a DNW (see also Figure 1d,g). b) Linear conductance G versus side gate voltages V_{g1} and V_{g2}. The nearly horizontal and vertical conductance lines reveal the transport resonance conditions for the two QDs controlled by the respective gates. c,d) Differential conductance dI/dV_{sd} versus bias V_{sd} and gate V_g of QD1 (QD2) along the horizontal (vertical) dashed lines in (b). The asterisks in (c,d) indicate, that the gate sweeps involve combinations of g1 and g2 according to the traces in (a). The maps show that both quantum dots are coupled to a common superconducting lead (gap $\Delta \approx 0.2$ meV). A small gate shift has occurred between measurement (b) and (c,d). e) Schematic of a S-DNW island with independent NW leads. The device geometry is similar to Figure 1e,h). f,g) Linear conductance G versus plunger gate V_{gate}. The plots show Coulomb blockade behavior for two pairs of electrodes, that is, upper nanowire (1-2) and interwire (4-1) hybrid nanowire transport. h) Bias spectroscopy showing Coulomb blockade diamonds related to transport through the S-island via leads 4-1. All measurements were performed at 30 mK.

step, it is possible to obtain a range of nanowire dimensions (Figure 5a) and also to realize more complex heterostructures such as the shadowed triplet structure seen in Figure 5d,e. In Figure 5c, we show that variations of the Au particle volume may be used to form nanowires with different dimensions and with that determine the overall morphology of the pairs. In turn, this can be a way to provide different transport characteristics of the two nanowires, for example, different numbers of 1D subbands in DNWs with two different diameters. In Figure 5e, the triplet structure is shifted slightly to one side so that one of the three nanowires is fully coated and the remaining two are half shadowed. Finally, Figure 5f showcases the feasibility of more complex structures, here exemplified by ten nanowires in a row.

5. Conclusions

In conclusion, the required DNW-superconductor hybrids have been successfully developed and can be grown with a high yield. The electrical transport has elucidated the inter-wire couplings and the properties of the DNW-superconductor hybrids. Focus has so far been on realizing Al/InAs-based DNWs by MBE, but the concepts can be transferred to other III-V methods and

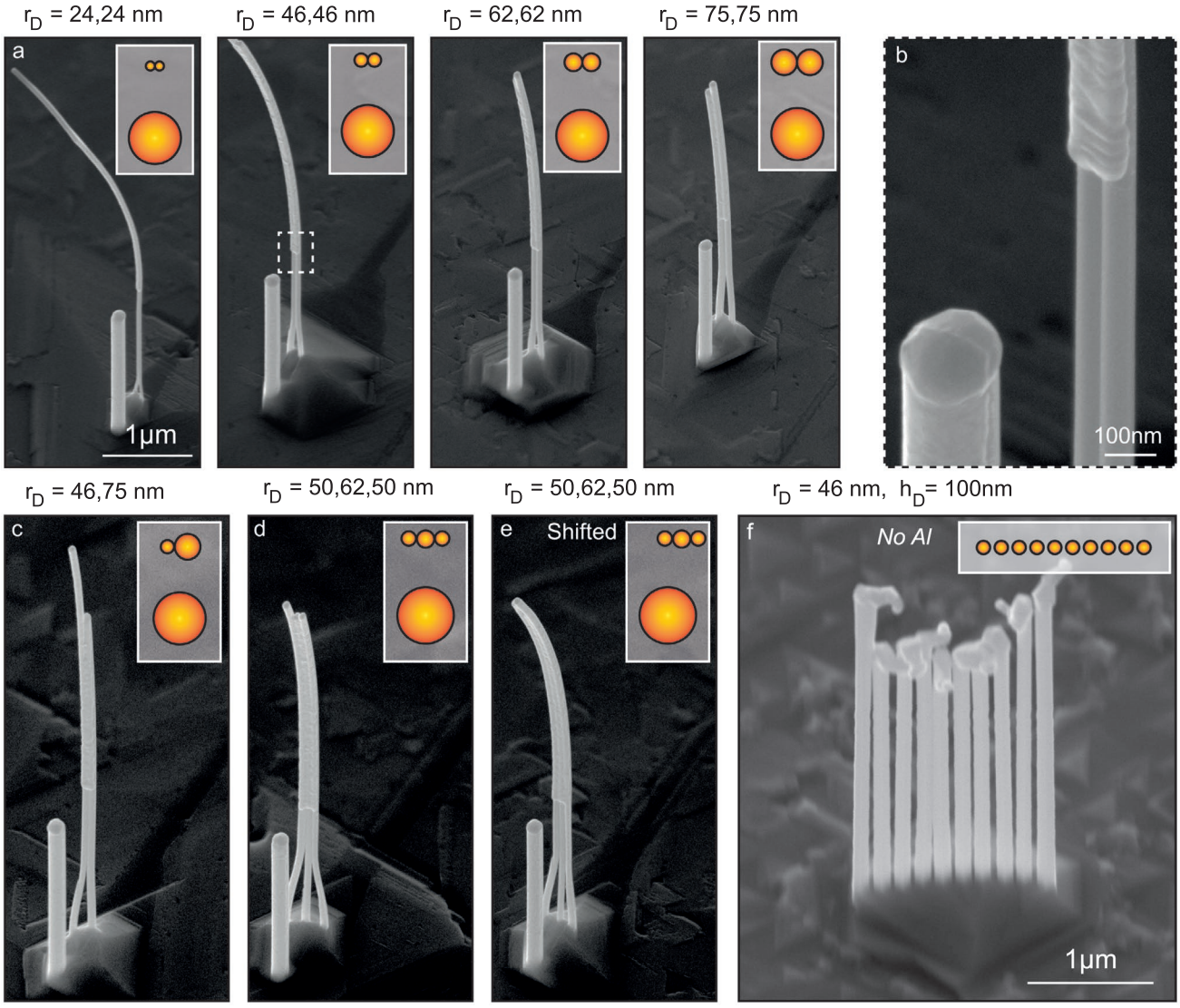

Figure 5. SEM micrographs of parallel nanowires in complex configurations. All nanowires were grown on the same wafer and all with ≈ 20 nm Al (except panel f). a) In situ shadowed parallel nanowires with varied dimensionality formed by different Au particle sizes. b) Zoom on the second panel in (a). The sharp shadow junction is visible as well as the rounded nanowires obtained by tuning the growth parameters. c) Parallel nanowire pair with different diameters. d) Three nanowires merged around the center nanowire that has an increasing diameter. e) Three nanowire bundle similar to (d), however shifted to ensure that one nanowire is not shadowed. f) Linear array of 10 parallel nanowires without metal coating.

materials that maintain an epitaxial relationship between the nanowires and the growth substrate, such as, for example, InSb and InP wires, as well as other growth systems that are also utilizing the VLS mechanism for nanowire growth, for example, metalorganic vapour phase epitaxy or chemical beam epitaxy. Likewise, the in situ approach used here will also allow for several different metal (superconductor) coatings and other in situ depositions, for example, of dielectrics or magnetic materials. Finally, DNWs can also be formed from NWs with axial heterostructures.

The parallel nanowire configurations demonstrated in this work matches the requirements for several proposals within hybrid superconductor-semiconductor devices, in particular experiments within the topological regime that cannot be performed with single hybrid nanowires. Moreover, DNWs could enable experiments on Coulomb drag induced supercurrents[50] in a system with low screening. Finally, bare multiwire arrangements with several parallel wires, based on structures shown in Figure 5f, mimic the setup proposed for studying the fractional quantum Hall effect in a quantum wire array.[51]

6. Experimental Section

EBL Defined Au Particles: To fabricate the initial Au catalyst particles used to grow nanowires in close proximity EI6/A4 resist was spun onto epi-ready InAs (111)B wafers. Precise openings in the resist were defined by making multiple electron beam exposures (shots), using a 100 keV Elionix ELS-7000 EBL system with a beam current of 500 pA and a dwell time of 200 µs/shot. After development (MIPK/IPA) and plasma ashing, the wafer was rinsed in a buffered HF solution for ≈20s. An Au thinfilm was deposited by an AJA electron beam evaporation

system at a rate of ≈1 Å s^{-1} and then lifted off in room temperature acetone. For more information about the EBL procedure, see Section S1, Supporting Information.

Nanowire Growth: Au catalyzed InAs nanowires were grown in a solid-source Varian GEN-II MBE system. To ensure a consistent growth environment, ≈1 µm of GaAs was grown on a GaAs calibration wafer before the wafers intended for nanowire growth were loaded in the MBE chamber. This ensured formation of type-I facets ($\{1\bar{1}00\}$) in case of sixfold symmetric nanowires. Different initial Au volumes and growth parameters were used to tune the dimensions of the InAs nanowires for the intended merging scheme. The effective V/III flux ratio used to grow the InAs nanowires shown in Figure 2 was ≈10 and for Figures 3 and 5, the ratio was ≈20. All nanowires were grown vertically using As_4 with a substrate thermocouple temperature of 447 °C. For more information, see Section S5, Supporting Information.

After growth of the InAs nanowires, the wafers were transferred through vacuum (≈10^{-10} Torr) to an attached metal deposition chamber. Here, the wafers were cooled to ~ –150 °C for ~ 3 h and aligned according to the electron beam evaporation source (see specifics in the main text). Al was evaporated as outlined in the main text with a rate of ≈3 Å s^{-1}.

Device Fabrication: Double nanowires with the desired geometries were identified by SEM microscopy and thereafter transferred to prepatterned device substrates using a micromanipulator under an optical microscope. It has been emphasized that in the case of type-II merged nanowires with a higher yield compared to type-I nanowires, the SEM step could be omitted. A standard EBL method was used to define Ti/Au contacts and gates (see Figure 1). Ar-ion milling was used prior to metal deposition to ensure Ohmic contact to the nanowires.

Supporting Information

Supporting Information is available from the Wiley Online Library or from the author.

Acknowledgements

This work was funded by the European Union's Horizon 2020 research and innovation programme QuantERA project no. 127900 (SuperTOP) and FETOpen grant no. 828948 (AndQC), the Carlsberg Foundation, the Niels Bohr Institute, the Villum Foundation project no. 25310, and the Ministry of Innovation and Technology and the NKFIH within the Quantum Information National Laboratory of Hungary and by the Quantum Technology National Excellence Program (Project Nr. 2017-1.2.1-NKP-2017- 00001), NKP-20-5 New National Excellence Program. The Center for Quantum Devices is supported by the Danish National Research Foundation. J.C.E.S. acknowledges funding from the European Union's Horizon 2020 research and innovation program under the Marie Sklodowska-Curie grant agreement No. 832645. The authors thank M. Aagesen, M. Burello, I. Nielsen, J. Paaske, G. Steffensen, M. Wauters, C.B. Sørensen, D. Laroche, D. Kjaer, O. Kurtossy, Z. Scherubl, C. Schrade, J. Sestoft, and P. Makk for assistance and discussions.

Conflict of Interest

The authors declare no conflict of interest.

Author Contributions

C.S., K.G.R., and J.N. conceived the in situ DNW concept; T.K., D.O., M.M., R.D.S., D.R., and J.N. developed growth schemes and performed structural characterizations; A.V., S.L., J.C.E.S., K.G.R., and J.N. performed transport measurements; J.N. supervised the project; T.K., K.G.R., and J.N. wrote the manuscript with input from all authors.

Data Availability Statement

Full data sets for all Figures, TEM images, transport data and other data that support the Findings of this study are openly available at https://doi.org/10.17894/ucph.d943422a-dfd7-4bf8-97a2-a56cd1e04e31.

Keywords

hybrid semiconductor-superconductor nanomaterials, parallel nanowires, quantum materials, semiconductor nanowires

Received: August 12, 2021
Revised: October 8, 2021
Published online: November 21, 2021

[1] F. Giustino, J. H. Lee, F. Trier, M. Bibes, S. M. Winter, R. Valentí, Y. W. Son, L. Taillefer, C. Heil, A. I. Figueroa, B. Plaçais, Q. S. Wu, O. V. Yazyev, E. P. Bakkers, J. Nygård, P. Forn-Díaz, S. de Franceschi, J. W. McIver, L. E. F. Torres, T. Low, A. Kumar, R. Galceran, S. O. Valenzuela, M. V. Costache, A. Manchon, E. A. Kim, G. R. Schleder, A. Fazzio, S. Roche, *J. Phys.: Mater.* **2021**, *3*, 42006.
[2] R. Aguado, *Appl. Phys. Lett.* **2020**, *117*, 240501.
[3] T. W. Larsen, K. D. Petersson, F. Kuemmeth, T. S. Jespersen, P. Krogstrup, J. Nygård, C. M. Marcus, *Phys. Rev. Lett.* **2015**, *115*, 127001.
[4] F. Luthi, T. Stavenga, O. W. Enzing, A. Bruno, C. Dickel, N. K. Langford, M. A. Rol, T. S. Jespersen, J. Nygård, P. Krogstrup, L. DiCarlo, *Phys. Rev. Lett.* **2018**, *120*, 100502.
[5] S. D. Sarma, M. Freedman, C. Nayak, *Quantum Inf.* **2015**, *1*, 15001.
[6] D. Aasen, M. Hell, R. V. Mishmash, A. Higginbotham, J. Danon, M. Leijnse, T. S. Jespersen, J. A. Folk, C. M. Marcus, K. Flensberg, J. Alicea, *Phys. Rev. X* **2016**, *6*, 31016.
[7] J. Klinovaja, D. Loss, *Phys. Rev. B* **2014**, *90*, 045118.
[8] B. Béri, N. R. Cooper, *Phys. Rev. Lett.* **2012**, *109*, 156803.
[9] A. Altland, R. Egger, *Phys. Rev. Lett.* **2013**, *110*, 196401.
[10] C. Schrade, M. Thakurathi, C. Reeg, S. Hoffman, J. Klinovaja, D. Loss, *Phys. Rev. B* **2017**, *96*, 035306.
[11] S. Plugge, A. Rasmussen, R. Egger, K. Flensberg, *New J. Phys.* **2017**, *19*, 012001.
[12] Z. X. Yang, N. Han, M. Fang, H. Lin, H. Y. Cheung, S. P. Yip, E. J. Wang, T. F. Hung, C. Y. Wong, J. C. Ho, *Nat. Commun.* **2014**, *5*, 5249.
[13] Z. Scherübl, A. Pályi, S. Csonka, *Beilstein J. Nanotechnol.* **2019**, *10*, 363.
[14] P. Krogstrup, N. L. B. Ziino, W. Chang, S. M. Albrecht, M. H. Madsen, E. Johnson, J. Nygård, C. M. Marcus, T. S. Jespersen, *Nat. Mater.* **2015**, *14*, 400.
[15] R. M. Lutchyn, E. Bakkers, L. P. Kouwenhoven, P. Krogstrup, C. Marcus, Y. Oreg, *Nat. Rev. Mater.* **2018**, *3*, 52.
[16] S. Gazibegovic, D. Car, H. Zhang, S. C. Balk, J. A. Logan, M. W. A. de Moor, M. C. Cassidy, R. Schmits, D. Xu, G. Wang, P. Krogstrup, R. L. M. O. het Veld, K. Zuo, Y. Vos, J. Shen, D. Bouman, B. Shojaei, D. Pennachio, J. S. Lee, P. J. van Veldhoven, S. Koelling, M. A. Verheijen, L. P. Kouwenhoven, C. J. Palmstrøm, E. P. A. M. Bakkers, *Nature* **2017**, *548*, 434.
[17] S. A. Khan, C. Lampadaris, A. Cui, L. Stampfer, Y. Liu, S. J. Pauka, M. E. Cachaza, E. M. Fiordaliso, J.-H. Kang, S. Korneychuk, T. Mutas, J. E. Sestoft, F. Krizek, R. Tanta, M. C. Cassidy, T. S. Jespersen, P. Krogstrup, *ACS Nano* **2020**, *14*, 14605.
[18] F. Krizek, T. Kanne, D. Razmadze, E. Johnson, J. Nygard, C. M. Marcus, P. Krogstrup, *Nano Lett.* **2017**, *17*, 6090.

[19] K. A. Dick, K. Deppert, M. W. Larsson, T. Mårtensson, W. Seifert, L. R. Wallenberg, L. Samuelson, *Nat. Mater.* **2004**, *3*, 380.
[20] K. D. M. Tornberg, S. Lehmann, *Appl. Phys. Lett.* **2018**, *113*, 123104.
[21] S. Baba, J. Sailer, R. S. Deacon, A. Oiwa, K. Shibata, K. Hirakawa, S. Tarucha, *Appl. Phys. Lett.* **2015**, *107*, 222602.
[22] S. Baba, C. Jünger, S. Matsuo, A. Baumgartner, Y. Sato, H. Kamata, K. Li, S. Jeppesen, L. Samuelson, H. Q. Xu, C. Schönenberger, S. Tarucha, *New J. Phys.* **2018**, *20*, 063021.
[23] K. Ueda, S. Matsuo, H. Kamata, S. Baba, Y. Sato, Y. Takeshige, K. Li, S. Jeppesen, L. Samuelson, H. Xu, S. Tarucha, *Sci. Adv.* **2019**, *5*, eaaw2194.
[24] O. Kürtössy, Z. Scherübl, G. Fülöp, I. E. Lukács, T. Kanne, J. Nygård, P. Makk, S. Csonka, *Nano Lett.* **2021**, *21*, 7929.
[25] A. Vekris, J. C. E. Saldaña, T. Kanne, M. Marnauza, D. Olsteins, F. Fan, X. Li, T. Hvid-Olsen, X. Qiu, H. Xu, J. Nygård, K. Grove-Rasmussen, *Phys. Rev. Res.* **2021**, *3*, 033240.
[26] A. Vekris, J. C. Estrada Saldaña, J. de Bruijckere, S. Lorić, T. Kanne, M. Marnauza, D. Olsteins, J. Nygård, K. Grove-Rasmussen, *Sci. Rep.* **2021**, *11*, 19034.
[27] M. H. Madsen, P. Krogstrup, E. Johnson, S. Venkatesan, E. Mühlbauer, C. Scheu, C. B. Sørensen, J. Nygård, *J. Cryst. Growth* **2013**, *364*, 16.
[28] T. Kanne, M. Marnauza, D. Olsteins, D. J. Carrad, J. E. Sestoft, J. de Bruijckere, L. Zeng, E. Johnson, E. Olsson, K. Grove-Rasmussen, J. Nygård, *Nat. Nanotechnol.* **2021**, *16*, 776.
[29] M. Bjergfelt, D. J. Carrad, T. Kanne, M. Aagesen, E. M. Fiordaliso, E. Johnson, B. Shojaei, C. J. Palmstrøm, P. Krogstrup, T. S. Jespersen, J. Nygård, *Nanotechnology* **2019**, *30*, 294005.
[30] R. Erdelyi, M. Madsen, G. Safran, Z. Hajnal, I. Lukacs, G. Fulop, S. Csonka, J. Nygård, J. Volk, *Solid State Commun.* **2012**, *152*, 1829.
[31] R. S. Deacon, A. Oiwa, J. Sailer, S. Baba, Y. Kanai, K. Shibata, K. Hirakawa, S. Tarucha, *Nat. Commun.* **2015**, *6*, 10299.
[32] W. G. van der Wiel, S. de Franceschi, J. M. Elzerman, T. Fujisawa, S. Tarucha, L. P. Kouwenhoven, *Rev. Mod. Phys.* **2002**, *75*, 1.
[33] R. S. Deacon, Y. Tanaka, A. Oiwa, R. Sakano, K. Yoshida, K. Shibata, K. Hirakawa, S. Tarucha, *Phys. Rev. Lett.* **2010**, *104*, 076805.
[34] E. J. H. Lee, X. Jiang, M. Houzet, R. Aguado, C. M. Lieber, S. de Franceschi, *Nat. Nanotechnol.* **2014**, *9*, 79.
[35] A. Jellinggaard, K. Grove-Rasmussen, M. H. Madsen, J. Nygård, *Phys. Rev. B* **2016**, *94*, 064520.
[36] M. R. Galpin, A. K. Mitchell, J. Temaismithi, D. E. Logan, B. Béri, N. R. Cooper, *Phys. Rev. B* **2014**, *89*, 045143.
[37] M. Papaj, Z. Zhu, L. Fu, *Phys. Rev. B* **2019**, *99*, 014512.
[38] A. P. Higginbotham, S. M. Albrecht, G. Kiršanskas, W. Chang, F. Kuemmeth, P. Krogstrup, T. S. Jespersen, J. Nygård, K. Flensberg, C. M. Marcus, *Nat. Phys.* **2015**, *11*, 1017.
[39] E. Gaidamauskas, J. Paaske, K. Flensberg, *Phys. Rev. Lett.* **2014**, *112*, 126402.
[40] J. Klinovaja, D. Loss, *Phys. Rev. B* **2014**, *90*, 045118.
[41] H. Ebisu, B. Lu, J. Klinovaja, Y. Tanaka, *Prog. Theor. Exp. Phys.* **2016**, *2016*, 8,083I01.
[42] C. Reeg, J. Klinovaja, D. Loss, *Phys. Rev. B* **2017**, *96*, 081301.
[43] M. Thakurathi, P. Simon, I. Mandal, J. Klinovaja, D. Loss, *Phys. Rev. B* **2018**, *97*, 045415.
[44] C. Schrade, L. Fu, *Phys. Rev. Lett.* **2018**, *120*, 267002.
[45] O. Dmytruk, M. Thakurathi, D. Loss, J. Klinovaja, *Phys. Rev. B* **2019**, *99*, 245416.
[46] P. Kotetes, M. T. Mercaldo, M. Cuoco, *Phys. Rev. Lett.* **2019**, *123*, 126802.
[47] A. Haim, Y. Oreg, *Phys. Rep.* **2019**, *825*, 1.
[48] M. Thakurathi, D. Chevallier, D. Loss, J. Klinovaja, *Phys. Rev. Res.* **2020**, *2*, 023197.
[49] D. J. Carrad, M. Bjergfelt, T. Kanne, M. Aagesen, F. Krizek, E. M. Fiordaliso, E. Johnson, J. Nygård, T. S. Jespersen, *Adv. Mater.* **2020**, *32*, 1908411.
[50] J.-M. Ji-Min Duan, S. Yip, *Phys. Rev. Lett.* **1993**, *70*, 3647.
[51] C. Kane, R. Mukhopadhyay, T. Lubensky, *Phys. Rev. Lett.* **2002**, *88*, 036401.